Insulating Ferromagnetic $LaCoO_{3-\delta}$ Films: A Phase Induced by Ordering of Oxygen Vacancies

Neven Biškup,[1,2] Juan Salafranca,[1,2,*] Virat Mehta,[3,4] Mark P. Oxley,[5,6] Yuri Suzuki,[3,4,7] Stephen J. Pennycook,[2,5] Sokrates T. Pantelides,[5,6,2] and Maria Varela[2,1]

[1]*Departamento de Física Aplicada III and Instituto Pluridisciplinar, Universidad Complutense de Madrid, Madrid 28010, Spain*
[2]*Materials Science and Technology Division, Oak Ridge National Laboratory, Oak Ridge, Tennessee 37831, USA*
[3]*Department of Material Science and Engineering, University of California, Berkeley, California 94720, USA*
[4]*Materials Sciences Division, Lawrence Berkeley National Laboratory, Berkeley, California 94720, USA*
[5]*Department of Physics and Astronomy, Vanderbilt University, Nashville, Tennessee 37235, USA*
[6]*Department of Electrical Engineering and Computer Science, Vanderbilt University, Nashville, Tennessee 37235, USA*
[7]*Department of Applied Physics and Geballe Laboratory for Advanced Materials, Stanford University, Stanford, California 94305, USA*

(Received 6 May 2013; revised manuscript received 24 September 2013; published 26 February 2014)

The origin of ferromagnetism in strained epitaxial $LaCoO_3$ films has been a long-standing mystery. Here, we combine atomically resolved *Z*-contrast imaging, electron-energy-loss spectroscopy, and density-functional calculations to demonstrate that, in epitaxial $LaCoO_3$ films, oxygen-vacancy superstructures release strain, control the film's electronic properties, and produce the observed ferromagnetism via the excess electrons in the Co *d* states. Although oxygen vacancies typically dope a material *n*-type, we find that ordered vacancies induce Peierls-like minigaps which, combined with strain relaxation, trigger a nonlinear rupture of the energy bands, resulting in insulating behavior.

DOI: 10.1103/PhysRevLett.112.087202 PACS numbers: 75.70.−i, 68.37.Ma, 79.20.Uv

In many strongly correlated oxide systems, several competing interactions are at play [1]. These include spin, charge, orbital, and lattice degrees of freedom. When these materials are synthesized in thin-film form, they may be constrained to have the same lattice parameter as the substrate. Epitaxial strain can enhance or suppress the diverse properties of complex oxides [2–6] and may also affect the delicate balance of the competing degrees of freedom, thus modifying the ground state. Lanthanum cobaltite ($LaCoO_3$ or LCO) epitaxial films under tensile strain have been considered a model system for understanding the stabilization of ground states not observed in bulk form [7–15]. While bulk LCO does not exhibit any long-range magnetic order, coherently strained LCO films are ferromagnetic (FM) at low temperatures [7,8]. Both bulk and thin-film samples are insulating, leading to the belief that the films are stoichiometric, because any substantial deviation from stoichiometry should lead to metallic behavior; e.g., oxygen vacancies should dope the material *n*-type.

Since the initial reports five years ago [7], several theoretical studies have tried to explain the insulating ferromagnetic state assuming stoichiometric films [16–20], but the predicted ground states are either ferromagnetic and metallic [16] or insulating with small or zero magnetization [19]. Recently, Choi *et al.* [21] reported atomically resolved *Z*-contrast images of LCO films on $SrTiO_3$ (STO) substrates, showing dark stripes that correspond to periodic La-La distances significantly larger than normal. On the basis of x-ray absorption and optical conductivity data, they inferred that the films are stoichiometric and, more specifically, that the dark stripes are not caused by oxygen vacancies, as in other Co oxides. They further proposed that large magnetic moments and ferromagnetic ordering are caused by the observed large atomic displacements in the stripes. Several issues, however, remain unresolved, especially the question of stoichiometry. Dark stripes have been observed in many complex oxide systems (cuprates, ferrites, cobaltites, etc.). Their definitive identification as oxygen-deficient planes was possible only by atomic-resolution electron-energy-loss spectroscopy [22–27]. Furthermore, theoretical calculations confirming that the observed atomic displacements are stable in the absence of vacancies are still lacking.

In this Letter, we use a combination of experimental data and theoretical calculations to demonstrate that oxygen-vacancy ordering is responsible for the ferromagnetic insulating state in epitaxial LCO thin films. We present atomically resolved *Z*-contrast images of LCO thin films grown on a (001) STO substrate, along with simultaneously collected, atomically resolved electron-energy-loss spectroscopy (EELS) and complementary chemical maps of the constituent elements. The EELS data demonstrate unambiguously that there is a significant oxygen deficiency, which is responsible for the lattice relaxation and the ensuing dark stripes in the *Z*-contrast images; it also results in charge ordering (CO) within the Co sublattice. We further report theoretical investigations of a model crystal structure with a periodic superstructure of oxygen

vacancies as deduced from the data. The calculated EELS in the O-depleted and stoichiometric regions are in agreement with the measured spectra, confirming the present conclusions. In the absence of vacancies, large La-La displacements are not stable. We find antiferromagnetically aligned high spin (HS) Co^{2+} states in the O-depleted planes and FM-ordered HS Co^{2+} ions in the stoichiometric planes, with a net magnetic moment per Co atom equal to $1\mu_B$, close to the measured values of $\sim 0.8\mu_B$ [13,17]. Finally, we show that, despite the oxygen-vacancy "doping," the film is insulating by an unusual mechanism: The ordered vacancies initially induce Peierls minigaps at several points in the Brillouin zone. A substantial relaxation ensues, leading to a nonlinear rupture of the energy bands with a sizable gap.

LCO films were grown on [100] STO substrates (all details regarding experiments and calculations are described in the Supplemental Material [28]). Figure 1(a) shows a Z-contrast image of a 14-nm-thick LCO film along the pseudocubic [100] zone axis, obtained in an aberration-corrected scanning transmission electron microscope. The intensity of every atomic column is approximately proportional to Z^2, so the heavier La columns are brightest. Lanthanum and cobalt atoms are clearly visible, while light O atoms are not. Periodic dark stripes are present. The La-La distance map and histogram are shown in Figs. 1(b) and 1(c), showing that dark stripes correspond to significantly dilated La-La distances ($\sim$4.5 versus $\sim$3.6 Å). The modulation vector of the superlattice lies in the plane of the interface, suggesting a strain release mechanism. Indeed, on average, the film has an in-plane lattice constant of 3.92 Å, closer to STO (3.905 Å) than to LCO bulk ($\sim$3.83 Å) [29]. In this work, we examine the physical origin of these stripes and their relationship with the magnetic properties.

The dark stripes in the Z-contrast images demonstrate the existence of a modulation in the structure but do not provide sufficient information about the stoichiometry. Thus, we turn to atomic-resolution EELS data for each element (Fig. 2). Despite the similar level of noise in the EELS signal for the three elements, the vertically averaged line intensities indicate that (i) the La and Co peaks have uniform height throughout the sample, suggesting no significant departure from stoichiometry for these elements in the stripe regions, and (ii) the O peaks are significantly reduced in the stripe regions. Simulated line intensities (see the Supplemental Material [28]) show that the data are reproduced *only* if large concentrations of O vacancies are present in the stripes. These results present the definitive conclusion that oxygen vacancies are present in the dark stripes.

The inset in Fig. 2 shows a map of the Co L_3/L_2 intensity ratio (ratio of the intensities of the main peaks in the Co L_3 and L_2 spectra). This ratio has been reported to increase with a decreased Co oxidation state [23,30] as in manganites [31]. The oxidation state accounts for the excess electrons in anion orbitals or the missing electrons in

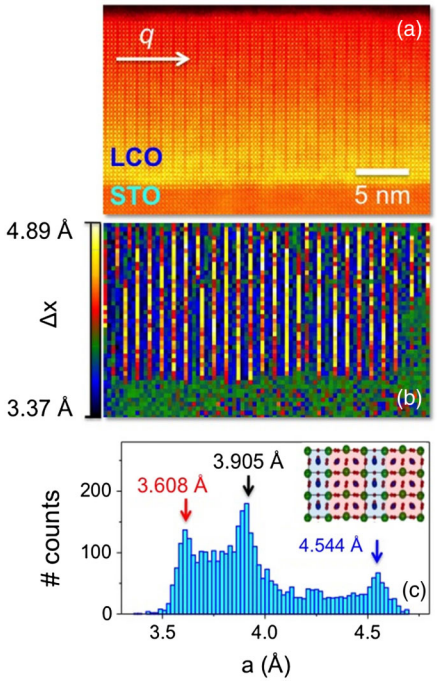

FIG. 1 (color online). (a) High resolution, high angle annular dark field (HAADF) image of a LCO thin film 15 nm thick, grown on a (001) oriented STO substrate, showing the contrast resulting from the O-vacancy ordering. The direction of the modulation vector, q, is marked with an arrow. (b) Map of the in-plane distance between first La neighbors (Δx) in (a), along the direction parallel to q. O-deficient planes are characterized by enlarged La-La distances. (c) Histogram of Δx values across the image. Three peaks are clearly observed: the one corresponding to the lattice parameter of the STO substrate (black arrow), the one from the LCO fully stoichiometric planes (red arrow), and the lattice distance corresponding to the O-deficient CoO_x planes (blue arrow). Inset: 2D projection of the structure along the [011] direction ([100] in the pseudocubic setting), marking oxygen-deficient (shaded blue) and stoichiometric (red) planes. Blue, red, and green spheres are Co, O, and La atoms, respectively.

cation orbitals that result from orbital hybridization. The Co L_3/L_2 ratio map shows that the Co oxidation state decreases in the dark stripes. Figure 3(a) shows a detailed L_3/L_2 ratio measurement from an EELS line scan and a modulation coinciding with the stripes. If Ref. [30] were used for calibration, this variation would correspond to a change in the average oxidation state of 0.4–0.7 electrons. However, dechanneling and the ensuing beam broadening result in a local L_3/L_2 ratio somewhat averaged between neighboring atomic planes, thus making a direct quantification difficult. Other origins for the modulation in the L_3/L_2 ratio cannot be dismissed *a priori*, but changes in the spin state [33] or crystallographic environment [34] of Co^{3+} have been shown before to produce much smaller changes in the L_3/L_2 ratio. Therefore, Figs. 2 and 3 exhibit fingerprints of a modulation of the occupancy of the Co $3d$ orbitals, which corresponds to a modulation of the nominal

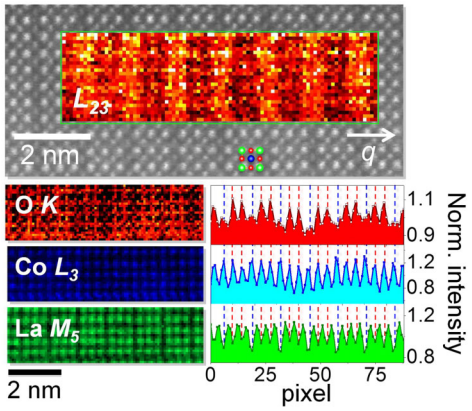

FIG. 2 (color online). Top: high resolution Z-contrast image of the LCO film showing an average modulation length of three perovskite blocks. The inset shows the Co L_3/L_2 intensity ratio map for a spectrum image acquired in the area marked with a green rectangle. A schematic shows the pseudocubic unit cell (blue = Co; green = La; red = O). Bottom left: elemental chemical maps constructed by integrating the corresponding EEL spectra: O K edge (red), Co L_3 edge (blue), and La M_5 edge (green). Bottom right: normalized intensity across the O K, Co L_3, and the La M_5 images on the left, vertically averaged across the whole images. Fully stoichiometric CoO_2 planes are indicated with red dashed lines in the background (through all three profiles), and O-deficient CoO_x planes are marked with blue dashed lines. The O intensity decreases on the latter planes as a result of the lower O content, which makes the La atoms move further apart from each other, giving rise to the dark stripes in the Z-contrast images.

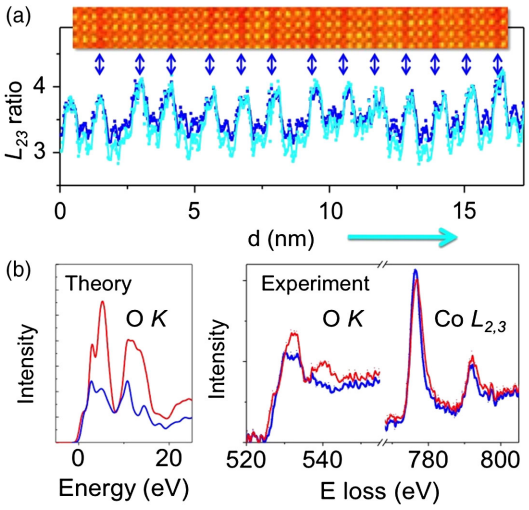

FIG. 3 (color online). EELS fine structures across the O-vacancy superlattice. (a) L_3/L_2 intensity ratio for an EELS line scan across the stripes, calculated by using a Hartree-Slater cross-section step function [27] (dark blue points), after deconvolution with the zero loss to remove multiple scattering, and also using the second derivative method [32] (cyan dots, same vertical scale). The top HAADF image in a matching scale shows the area where the line scan was acquired. Blue arrows mark the position of the O-deficient planes. (b) Theoretical O K absorption edge along with experimental O K and Co $L_{2,3}$ edges [averaged from the line scan in (a)] for the fully oxygenated CoO_2 planes (red) and the O-deficient planes (blue).

Co oxidation state, often called charge ordering (CO) [35,36]. The presence of CO is surprising, because these LCO films are ferromagnetic (CO is usually associated with antiferromagnetism). Only on very rare occasions do ferromagnetic systems exhibit CO [37,38].

The observed CO is a result of the oxygen deficiency in the dark stripes. Averaged O K and Co $L_{2,3}$ spectra from the dark stripes (blue) and the bright CoO_2 planes (red) are shown in Fig. 3(b). The prepeak feature at the onset of the edge (527 eV) and the main peaks (532 and 540 eV) are strongly suppressed in the dark stripes, and the intensity is reduced in the continuum region of the spectrum. This observation confirms that O deficiency exists in the dark stripes, not just disorder. In addition, if the O concentration in the dark stripes were the same as in the bright stripes, we would see an *increase* in O signal (see the Supplemental Material [28]), as fewer electrons are scattered out of the beam from the dark stripes than from the bright planes.

In order to examine the electronic and magnetic properties of the oxygen-deficient strained LCO films, we carried out calculations based on density-functional theory (DFT) using a model crystal structure (Fig. 4). Electron-electron correlations are included by a Hubbard-like interaction [39] with $U = 3.7$ eV [17–19]. The in-plane dimensions of the unit cell are constrained to integer multiples of the STO substrate. After an epitaxially constrained structural relaxation, the resulting atomic structure contains two distinct Co sites: Co atoms in O-vacancy-rich (CoO_x) planes have a distorted *tetrahedral* environment, while Co atoms in stoichiometric CoO_2 planes have an octahedral environment. Such coexistence of tetrahedral and octahedral crystallographic positions has been previously observed in the brownmillerite-type structures of Sr-doped cobaltites [24,40,41]. The chemical formula of the unit cell is $La_6Co_6O_{16}$, and the average O deficiency is 11%.

Using the above structure, we calculated the O K spectra in both the O-deficient and the stoichiometric regions [Fig. 3(b)]. The prepeak is lower in the O-deficient regions. In the presence of O vacancies, electrons fill some of the otherwise available final states with $O-p/Co-d$ orbital content. La-La distance dilation produces a smaller hybridization between $O-2p$ and $La-d$ orbitals, and a decrease of intensity of the 6-eV peak. Finally, the 15-eV peak arises from hybridization with $Co-p$ levels, and it is reduced in the O-deficient planes because of changes in coordination. These fine-structure changes are in excellent agreement with the experimental spectra, confirming the conclusion that the dark stripes in the Z-contrast images are O deficient.

Our conclusion that the dark stripes have a substantial oxygen deficiency is in disagreement with previous work by Choi *et al.* [21]. These authors reported similar dark stripes in epitaxial LCO films but concluded that their thin films are stoichiometric by comparing x-ray absorption

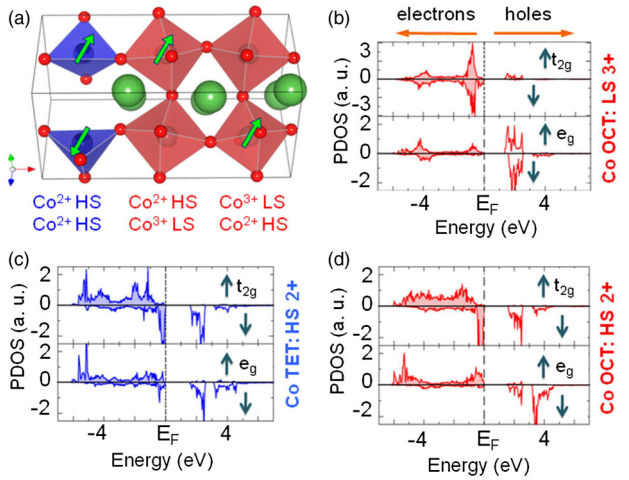

FIG. 4 (color online). The 3D model of the structure, and oxidation and spin states. Oxygen ions (red spheres) form distorted tetrahedra (blue) around Co ions (dark blue spheres) in vacancy-rich planes and bulklike octahedra (red) around Co atoms in fully oxygenized planes. Large green arrows indicate a high spin state and its relative direction (*up* or *down*). (b) Calculated density of states projected over different Co ions: high spin Co^{2+} in tetrahedral environment (top); high spin Co^{2+} in octahedral environment (middle); low spin Co^{3+} in a similar octahedral environment (bottom). Calculation details are in the Supplemental Material [28] (see also Refs. [40–43]).

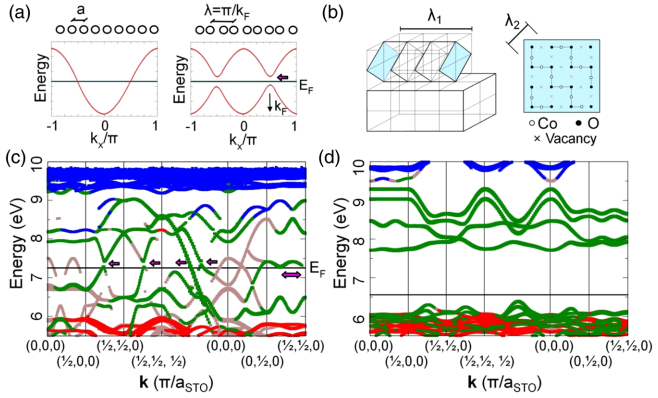

FIG. 5 (color online). Origin of the energy gap. (a) Peierls mechanism. In a metallic 1D undistorted system (left), a distortion with a periodicity equal to half the Fermi wavelength ($\lambda = \pi/k_F$) opens a gap, marked by the arrow (right). (b) Atomic structure of $LaCoO_{3-\delta}$ thin films on $SrTiO_3$ substrates. $\lambda_{1,2}$ indicate periodicities induced by the O-vacancy ordering. (c), (d) Band diagram of the majority spin states, projected into the $LaCoO_3$, reduced Brillouin zone: ferromagnetic undistorted material (c) and magnetic and structurally relaxed system (d). Colors indicate orbital character: *s* and *p* (light brown), t_{2g} (red), e_g (green), and *f* (blue). Arrows mark Peierls-like gaps.

spectroscopy and optical conductivity with corresponding data in bulk LCO. Such data, however, are macroscopic, averaging over the entire sample, and do not provide an unambiguous signature of what happens in the dark stripes. We should point out that, prior to the publication of Ref. [21]], some of the coauthors of that paper published atomically resolved EELS [42], which, like our data, show a definite reduction of the O *K* EELS in the stripes relative to EELS away from the stripes.

To determine the spin and oxidation state, we analyzed the occupied and empty states in the calculations. We assigned oxidation states based on the different Co-projected density of states (Fig. 4), as described in the Supplemental Material [28]. Tetrahedral Co atoms in the O-deficient stripes are in a 2+, HS state; all the spin *up* *d* orbitals are filled because intra-atomic exchange interaction dominates. These tetrahedral Co atoms are ordered anti-FM, thus not contributing to the net magnetization. Half of the Co atoms adjacent to the stripes, surrounded by O octahedra, are also HS Co^{2+}, but FM-ordered. These Co atoms are arranged in a checkerboard pattern with bulklike low-spin (LS) Co^{+3} atoms (Fig. 4) resulting in a net magnetic moment of $1\mu_B$/Co (experiments find $\sim 0.8\mu_B$) [13]. We attribute the FM coupling to a superexchangelike hybridization of HS Co^{2+} e_g electrons through the LS Co^{+3} atoms.

Finally, we address the issue of why, despite the electron doping arising from the vacancies, both theory and experiment find an insulating behavior. Calculations show that the gap is induced by the ordering of the vacancies, associated with a Peierls-like mechanism [Fig. 5(a)]. This mechanism is not believed to occur in 3D where bands cross the Fermi surface at various places. We carried out DFT calculations of the energy bands of LCO in the perovskite crystal structure, strained by lattice mismatch to STO. After insertion of the vacancies as in Fig. 5(b), the calculated energy bands for the spin-majority electrons are shown in Fig. 5(c). Although Peierls-like minigaps arise at several points in the Brillouin zone, bands also cross the Fermi energy at other points, and the system remains metallic. When we allowed the system to relax, however, a nonlinear relaxation occurs, and the energy bands truly rupture (beyond the usual, Peierls, linear energy gain), leading to the opening of a large energy gap [Fig. 5(d)]. Increasing or decreasing the number of vacancies within the same unit cell by one affects the magnitude of the gap but does not close it. However, if the ordering is significantly altered by placing the vacancies in different crystallographic sites, a metallic state results. In addition to the relaxation, the magnetization changes from $2.1\mu_B$/Co to $1\mu_B$/Co, consistent with experiments [13]. Thus, oxygen-vacancy ordering, lattice relaxation (which accommodates strain), and spin interactions work synergistically to lower the energy and produce the observed phenomena.

In conclusion, we have shown that LCO films under tensile strain relax by generating oxygen-vacancy superstructures that control the structural, electronic, and magnetic properties. These phenomena may occur in other materials providing a new, important degree of freedom to custom design thin-film properties.

N. B. and J. S. contributed equally to this work. The authors thank Masashi Watanabe for the Digital Micrograph PCA plug-in and C. Leighton for fruitful discussions (M. V.). Research at ORNL (S. J. P. and M. V.) was supported by the U.S. Department of Energy (DOE), Basic Energy Sciences (BES), Materials Sciences and Engineering Division, and through a user project supported by ORNL's Shared Research Equipment (ShaRE) User Program, which is also sponsored by DOE-BES. Research at UCM (N. B. and J. S.) was supported by the ERC starting Investigator Award, Grant No. 239739 STEMOX, Fundación Caja de Madrid, and Juan de la Cierva program (J. S.). Research at UC Berkeley/LBNL and Stanford was supported by the Director, Office of Science, Office of Basic Energy Sciences, Division of Materials Sciences and Engineering under Contracts No. DE-AC02-05CH11231 and No. DE-SC0008505, respectively. Research at Vanderbilt was supported in part by the U.S. DOE Grant No. DE-FG02-09ER46554 and the McMinn Endowment. Computations were supported by the National Center for Supercomputing Applications (U.S. Department of Energy, Contract No. DE-AC02-05CH11231).

*Corresponding author.jsalafra@ucm.es

[1] E. Dagotto, Science **318**, 1076 (2007).
[2] Y. Tokura and N. Nagaosa, Science **288**, 462 (2000).
[3] K. H. Ahn, T. Lookman, and A. R. Bishop, Nature (London) **428**, 401 (2004).
[4] R. J. Zeches *et al.*, Science **326**, 977 (2009).
[5] M. Dawber, K. M. Rabe, and J. F. Scott, Rev. Mod. Phys. **77**, 1083 (2005).
[6] A. Llordés *et al.*, Nat. Mater. **11**, 329 (2012).
[7] D. Fuchs, C. Pinta, T. Schwarz, P. Schweiss, P. Nagel, S. Schuppler, R. Schneider, M. Merz, G. Roth, and H. v. Löhneysen, Phys. Rev. B **75**, 144402 (2007).
[8] V. V. Mehta, M. Liberati, F. J. Wong, R. Vilas Chopdekar, E. Arenholz, and Y. Suzuki, J. Appl. Phys. **105**, 07E503 (2009).
[9] A. Herklotz, A. D. Rata, L. Schultz, and K. Dörr, Phys. Rev. B **79**, 092409 (2009).
[10] J. W. Freeland, J. X. Ma, and J. Shi, Appl. Phys. Lett. **93**, 212501 (2008).
[11] D. Fuchs, E. Arac, C. Pinta, S. Schuppler, R. Schneider, and H. v. Löhneysen Phys. Rev. B **77**, 014434 (2008).
[12] A. D. Rata, A. Herklotz, L. Schultz, and K. Dörr, Eur. Phys. J. B **76**, 215 (2010).
[13] M. Merz, P. Nagel, C. Pinta, A. Samartsev, H. v. Löhneysen, M. Wissinger, S. Uebe, A. Assmann, D. Fuchs, and S. Schuppler, Phys. Rev. B **82**, 174416 (2010).
[14] J. B. Goodenough, J. Phys. Chem. Solids **6**, 287 (1958).
[15] M. A. Señaris-Rodriguez and J. B. Goodenough, J. Solid State Chem. **116**, 224 (1995).
[16] J. M. Rondinelli and N. A. Spaldin, Phys. Rev. B **79**, 054409 (2009).
[17] A. Posadas, M. Berg, H. Seo, A. de Lozanne, A. A. Demkov, D. J. Smith, A. P. Kirk, D. Zhernokletov, and R. M. Wallace, Appl. Phys. Lett. **98**, 053104 (2011).
[18] H. Hsu, P. Blaha, and R. M. Wentzcovitch, Phys. Rev. B **85**, 140404(R) (2012).
[19] H. Seo, A. Posadas, and A. A. Demkov, Phys. Rev. B **86**, 014430 (2012). Both Refs. [17] and [18] actually obtained almost identical insulating states with a magnetization of $\approx 2\mu_B/\mathbf{Co}$; but Ref. [19] demonstrates that a bigger unit cell allows for a similar state with an antiparallel (net magnetization $0\mu_B/\mathbf{Co}$) or slightly canted ($0.25\mu_B/\mathbf{Co}$) spin arrangement.
[20] J. Fujioka, Y. Yamasaki, H. Nakao, R. Kumai, Y. Murakami, M. Nakamura, M. Kawasaki, and Y. Tokura, Phys. Rev. Lett. **111**, 027206 (2013).
[21] W. S. Choi *et al.*, Nano Lett. **12**, 4966 (2012).
[22] C. Chaillout, M. Alario-Franco, J. Capponi, J. Chenavas, J. Hodeau, and M. Marezio, Phys. Rev. B **36**, 7118 (1987).
[23] R. F. Klie, Y. Ito, S. Stemmer, and N. D. Browning, Ultramicroscopy **86**, 289 (2001).
[24] J. Gazquez, W. Luo, M. P. Oxley, M. Prange, M. A. Torija, M. Sharma, C. Leighton, S. T. Pantelides, S. J. Pennycook, and M. Varela, Nano Lett. **11**, 973 (2011).
[25] W. Dachraoui, J. Hadermann, A. M. Abakumov, A. A. Tsirlin, D. Batuk, K. Glazyrin, C. McCammon, L. Dubrovinsky, and G. Van Tendeloo, Chem. Mater. **24**, 1378 (2012).
[26] Y. Ito, R. F. Klie, N. D. Browning, and T. J. Mazanec, J. Am. Ceram. Soc. **85**, 969 (2002).
[27] Y.-M. Kim, J. He, M. D. Biegalski, H. Ambaye, V. Lauter, H. M. Christen, S. T. Pantelides, S. J. Pennycook, S. V. Kalinin, and A. Y. Borisevich, Nat. Mater. **11**, 888 (2012).
[28] See Supplemental Material at http://link.aps.org/supplemental/10.1103/PhysRevLett.112.087202 for details.
[29] P. G. Radaelli and S.-W. Cheong, Phys. Rev. B **66**, 094408 (2002).
[30] Z. L. Wang, J. S. Yin, and Y. D. Jiang, Micron **31**, 571 (2000).
[31] M. Varela, M. Oxley, W. Luo, J. Tao, M. Watanabe, A. Lupini, S. Pantelides, and S. Pennycook, Phys. Rev. B **79**, 085117 (2009).
[32] G. A. Botton, C. C. Appel, A. Horsewell, and W. M. Stobbs, J. Microsc. **180**, 211 (1995).
[33] R. F. Klie, J. Zheng, Y. Zhu, M. Varela, J. Wu, and C. Leighton, Phys. Rev. Lett. **99**, 047203 (2007).
[34] S. Turner, J. Verbeeck, F. Ramezanipour, J. E. Greedan, G. Van Tendeloo, and G. A. Botton, Chem. Mater. **24**, 1904 (2012).
[35] W. Luo, A. Franceschetti, M. Varela, J. Tao, S. Pennycook, and S. Pantelides, Phys. Rev. Lett. **99**, 036402 (2007).
[36] H. Raebiger, S. Lany, and A. Zunger, Nature (London) **453**, 763 (2008).
[37] J. C. Loudon, N. D. Mathur, and P. A. Midgley, Nature (London) **420**, 797 (2002).
[38] P. Mahadevan, A. Kumar, D. Choudhury, and D. D. Sarma, Phys. Rev. Lett. **104**, 256401 (2010).
[39] S. L. Dudarev, G. A. Botton, S. Y. Savrasov, C. J. Humphreys, and A. P. Sutton, Phys. Rev. B **57**, 1505 (1998).
[40] M. T. Anderson, J. T. Vaughey, and K. R. Poeppelmeier, Chem. Mater. **5**, 151 (1993).
[41] T. G. Parsons, H. D'Hondt, J. Hadermann, and M. A. Hayward, Chem. Mater. **21**, 5527 (2009).
[42] J. H. Kwon *et al.* in *Proceedings of APMC 10/ICONN 2012/ACMM 22, Perth, Australia, 2012*, http://www.microscopy.org.au/ACMM-22/ACMM-APMC-ICONN.zip.
[43] P. E. Blöchl, Phys. Rev. B **50**, 17953 (1994).